Note: This copy is for your personal, non-commercial use only. To order presentation-ready copies for distribution to your colleagues or clients, contact us at www.rsna.org/rsnarights.



Radiology

# Brain MR Imaging at Ultra-low Radiofrequency Power[1]

Subhendra N. Sarkar, PhD
David C. Alsop, PhD
Ananth J. Madhuranthakam, PhD
Reed F. Busse, PhD
Philip M. Robson, PhD
Neil M. Rofsky, MD
David B. Hackney, MD

**Purpose:** To explore the lower limits for radiofrequency (RF) power–induced specific absorption rate (SAR) achievable at 1.5 T for brain magnetic resonance (MR) imaging without loss of tissue signal or contrast present in high-SAR clinical imaging in order to create a potentially viable MR method at ultra-low RF power to image tissues containing implanted devices.

**Materials and Methods:** An institutional review board–approved HIPAA-compliant prospective MR study design was used, with written informed consent from all subjects prior to MR sessions. Seven healthy subjects were imaged prospectively at 1.5 T with ultra-low–SAR optimized three-dimensional (3D) fast spin-echo (FSE) and fluid-attenuated inversion-recovery (FLAIR) T2-weighted sequences and an ultra-low–SAR 3D spoiled gradient-recalled acquisition in the steady state T1-weighted sequence. Corresponding high-SAR two-dimensional (2D) clinical sequences were also performed. In addition to qualitative comparisons, absolute signal-to-noise ratios (SNRs) and contrast-to-noise ratios (CNRs) for multicoil, parallel imaging acquisitions were generated by using a Monte Carlo method for quantitative comparison between ultra-low–SAR and high-SAR results.

**Results:** There were minor to moderate differences in the absolute tissue SNR and CNR values and in qualitative appearance of brain images obtained by using ultra-low–SAR and high-SAR techniques. High-SAR 2D T2-weighted imaging produced slightly higher SNR, while ultra-low–SAR 3D technique not only produced higher SNR for T1-weighted and FLAIR images but also higher CNRs for all three sequences for most of the brain tissues.

**Conclusion:** The 3D techniques adopted here led to a decrease in the absorbed RF power by two orders of magnitude at 1.5 T, and still the image quality was preserved within clinically acceptable imaging times.

© RSNA, 2011

[1] From the Department of Radiology, Beth Israel Deaconess Medical Center, Harvard Medical School, 330 Brookline Ave, Boston, MA 02215 (S.N.S., D.C.A., P.M.R., N.M.R., D.B.H.); Applied Science Laboratory, GE Healthcare, Boston, Mass (A.J.M.); and Applied Science Laboratory, GE Healthcare, Madison, Wis (R.F.B.). Received December 23, 2009; revision requested February 12, 2010; final revision received June 18; accepted August 26; final version accepted December 20. **Address correspondence to** S.N.S. (e-mail: *ssarkar@bidmc.harvard.edu*).

© RSNA, 2011

Fast spin-echo (FSE) imaging with T2-weighted and fluid-attenuated inversion-recovery (FLAIR) sequences is an integral part of clinical brain magnetic resonance (MR) imaging. These methods are also specific absorption rate (SAR) for radiofrequency (RF) power–intensive, mainly because of the multiple refocusing pulses used. High-spatial-resolution three-dimensional (3D) FSE sequences are increasingly appealing for brain imaging after substantial improvements have been made in preserving spin-echo image contrast (1,2) within clinically feasible imaging times (3,4). Reduction of SAR in FSE MR sequences can be achieved by reducing the flip angles of the refocusing pulses (4–7). A substantial reduction of power is possible with this approach (4), and yet, remarkably low refocusing flip angles do not adversely affect the inherent tissue contrast or signal-to-noise ratio (SNR) (8). Reduced flip angles have been used to reduce SAR to acceptable levels at a high field strength and to control the blurring in long–echo train imaging (5,9). With parallel imaging (10), the number of echoes can also be reduced and, hence, SAR. However, researchers in none of these studies had SAR reduction below standard safety guidelines as the primary goal.

We sought to determine whether SAR can be drastically reduced by using existing clinical imagers to create a large margin to account for interimager RF power variability and possible errors in SAR measurements in order to minimize MR imaging heating risk in patients while approximately preserving image quality and tissue contrast. In this work, modified 3D techniques were adopted to decrease SAR dramatically (to an ultra-low level) without loss of image quality. We define *ultra-low RF power* as one that is 100 times lower than Food and Drug Administration guidelines for whole-body average SAR in healthy subjects, or 0.04 W/kg. Such an ultra-low–power MR imaging approach may help device manufacturers to pursue MR imaging safety without sacrificing diagnostic quality if the higher, standard SAR levels are contraindicated, particularly at higher field strengths at which RF heating may further limit imaging acquisition choices.

The specific purpose of this work was to explore the lower limits for RF power–induced SAR achievable at 1.5 T for brain MR imaging without loss of tissue signal or contrast present in high-SAR clinical imaging in order to create a potentially viable MR method at ultra-low RF power to image tissues containing implanted devices. Although, for most images obtained with clinical MR imaging units, RF power deposition can be carefully controlled to be within Food and Drug Administration limits, the dangers of RF power can increase when conductors or electronics are implanted or are in close proximity to the patient. Therefore, the task of RF power reduction to such an ultra-low level was undertaken to develop one of the lowest RF power methods that can minimize the dangers of RF power deposition and, hence, may potentially offer a safer approach to extend MR compatibility to image tissues containing implanted devices.

## Advance in Knowledge

- Three-dimensional fast spin-echo and gradient-echo techniques with optimized radiofrequency (RF) pulses, lower flip angles, and stretched pulse widths permitted approximately 100-fold reduction in specific absorption rate (SAR) for RF power while diagnostic-quality brain MR images were obtained.

## Implications for Patient Care

- By using ultra-low–SAR brain MR imaging at 1/100th of the routine, clinical SAR levels, diagnostic-quality brain images with traditional MR tissue contrast can be obtained within clinical imaging times.
- When pursuing advanced MR techniques such as newer RF coils and higher-field-strength magnets for imaging patients, the presented ultra-low–SAR approach offers the potential to help minimize RF power constraints.

## Materials and Methods

Two authors are employees of GE Healthcare (A.J.M. [Boston, Mass] and R.F.B. [Madison, Wis]). They provided the initial research pulse sequence and collaborated in the technical aspects of the sequence and the manuscript but were not involved in the clinical aspects of the study design or interpretation of results. The institutional authors, who are not employees of GE Healthcare, were in control of all data and information submitted for publication. None of the institutional authors received a consulting fee.

### Subjects

We used an institutional review board–approved Health Insurance Portability and Accountability Act–compliant prospective MR study design, with written informed consent from all subjects prior to MR sessions. The 3D sequence parameters were optimized by testing the 3D FSE sequences with phantoms and with three subjects who functioned

**Published online before print**
10.1148/radiol.11092445

**Radiology 2011;** 259:550–557

**Abbreviations:**
CC WM = corpus callosal WM
CNR = contrast-to-noise ratio
CSF = cerebrospinal fluid
FLAIR = fluid-attenuated inversion recovery
FSE = fast spin echo
GM = gray matter
RF = radiofrequency
SAR = specific absorption rate
SNR = signal-to-noise ratio
SPGR = spoiled gradient-recalled acquisition in the steady state
3D = three-dimensional
2D = two-dimensional
WM = white matter

**Author contributions:**
Guarantors of integrity of entire study, S.N.S., A.J.M.; study concepts/study design or data acquisition or data analysis/interpretation, all authors; manuscript drafting or manuscript revision for important intellectual content, all authors; approval of final version of submitted manuscript, all authors; literature research, S.N.S., D.C.A., N.M.R., D.B.H.; clinical studies, D.B.H.; experimental studies, S.N.S., A.J.M.; statistical analysis, S.N.S.; and manuscript editing, S.N.S., D.C.A., A.J.M., N.M.R., D.B.H.

See Materials and Methods for pertinent disclosures.

**Table 1**

**Acquisition Parameters for Clinical 2D High-SAR and Optimized 3D Ultra-low–SAR Sequences at 1.5 T**

| Sequence* | Time | Section Thickness and Gap (mm) and No. of Sections | Acquisition Time (min:sec) and Acceleration Factor | Echo Train Length and Bandwidth (kHz) | Excitation and Refocusing Flip Angles (degrees) | Average Whole-Body SAR (W/kg) |
|---|---|---|---|---|---|---|
| T2 FSE | | | | | | |
| 2D high SAR | 3200/81† | 4.8, 1.6, 18 | 3:19, 1 | 12, ± 25 | 90, 180 | 2.1 |
| 3D ultra-low SAR | 5000/73† | 1.6, 0, 112 | 8:31, 2.8 | 70, ± 83.3 | 90; 120 for first, 35 for minimum, 45 for center, 60 for last | 0.02 |
| T2 FLAIR FSE | | | | | | |
| 2D high SAR | 10000/114/2250‡ | 4.8, 1.6, 18 | 4:00, 1 | 10, ± 31.2 | 90, 180 | 1.1 |
| 3D ultra-low SAR | 8000/130/2275‡ | 1.6, 0, 112 | 10:35, 2.8 | 90, ± 25 | 90; 120 for first, 35 for minimum, 45 for center, 60 for last | 0.03 |
| T1 2D high-SAR spin-echo | 417/14† | 4.8, 1.6, 18 | 3:13, 1 | 1, ± 15.6 | 90, 180 | 1.6 |
| T1 3D ultra-low–SAR SPGR | 30/5.5† | 1.6, 0, 112 | 4:02, 2.7 | 1, ± 15.6 | 20, . . . | 0.02 |

Note.—SPGR = spoiled gradient-recalled acquisition in the steady state, T1 = T1 weighted, T2 = T2 weighted.

* For all sequences, acquisition was in the sagittal plane, and a 24 × 24 cm$^2$ sagittal field of view and acquisition matrix of 256 × 224 reconstructed to 512 × 512 matrix were used.

† Values are repetition time (msec)/echo time, effective (msec).

‡ Values are repetition time (msec/echo time, effective (msec)/inversion time (msec).

as healthy control subjects, according to the study design devised by three authors (S.N.S., D.C.A., D.B.H.). The optimized brain MR sequences were then applied in seven consecutive healthy subjects with no implanted hardware or other devices (four women, three men; age range, 29–67 years).

## Imaging and SAR Calculation

All imaging was performed with a 1.5-T MR imager (HDx; GE Healthcare, Milwaukee, Wis) by using an eight-channel receive-only head coil with a body coil for transmission. The total session time was 55 minutes for each subject, including three ultra-low–SAR 3D sequences, three high-SAR clinical two-dimensional (2D) sequences, and six background noise images for computing absolute SNR maps. The 3D and 2D imaging results were compared quantitatively by using absolute local SNR and CNR values and were also qualitatively evaluated for overall image quality, including fine structures and artifacts.

All SAR values reported in Table 1 were whole-body average SAR values, as estimated from the vendor's whole-body SAR calculation algorithm. Calibration of the SAR calculation model has been performed by the manufacturer empirically for rectangular pulses by means of comparison with power measurements across a range of subjects (11). Although the exact relationship between local and whole-body SAR is not known, local SAR and, therefore, the risk of local tissue heating can be minimized by minimizing the whole-body SAR. Note that a more rigorous way to estimate local SAR values for low-SAR sequences would be with calorimetric power measurements in the bore of the imager, which was not pursued in the current study. Any such measurement will depend on experimental geometry and model tissue materials used.

## Simulation

For the RF-modulated 3D FSE sequence (described below), simulations were performed (R.F.B., A.J.M.) for expected MR signal and related tissue contrast levels as a function of the refocusing echo train for various tissues (Fig 1) and were used for optimization of imaging parameters for 3D FSE T2-weighted and 3D FLAIR T2-weighted sequences (S.N.S., A.J.M.) (4). No simulation was performed to predict the signal behavior for the 3D SPGR T1-weighted sequence.

## Low-SAR T2-weighted MR Sequence

We employed a 3D fast recovery fast spin-echo–based T2-weighted research sequence (a development version similar to single-slab 3D FSE [Cube; GE Healthcare, Milwaukee, Wis]) with options for control of refocusing flip angles (4). A long repetition time to lower global SAR was used but with long echo trains to gain time efficiency. To counter the excess SAR generated by the long train of refocusing pulses, we used an optimized refocusing pulse-modulation scheme (4,6) but with lower than usual refocusing flip angles. We also reduced the refocusing RF power by stretching the pulse widths by threefold (to 1.0 msec) because RF pulse power is inversely proportional to the pulse duration. Though these longer pulses are slightly more sensitive to frequency offset and susceptibility, they are still much shorter and, consequently, more robust to these effects than are RF pulses used in most clinical sequences. A 3D slab-selective 90° pulse was used for excitation, while nonselective RF pulses were used for refocusing. The SAR was also reduced by efficiently filling the missing k-space data with a 2D autocalibrating reconstruction for Cartesian sampling

Radiology

parallel imaging algorithm (10) applied along two phase-encoding directions, with a net acceleration factor of 2.8. The imaging parameters are presented in Table 1. Linear-modulation view ordering was chosen that skips corners of k-space, further reducing the SAR and imaging time. Note that similar steps for modifying 3D pulse sequences can be implemented with imagers from other vendors, and they should achieve substantial power reduction, although the exact degree of SAR reduction will depend somewhat on the details of vendor sequence implementation.

Figure 1 shows the pulse-modulation scheme that was followed by lowering the refocusing flip angles from an initial value (flip angle, or $\alpha_{first}$, of 120°) to a minimum (or $\alpha_{min}$) to establish a pseudo–steady state followed by a slowly varying, small increase to compensate for tissue T2 decay. A higher value of the minimum flip angle ($\alpha_{min}$) was found to increase SNR, image blurring, and sequence SAR, while 35° was found to be optimum. Refocusing pulses after reaching the pseudo–steady state constitute a majority of the SAR-producing pulses and a slight increase (to a final value, or $\alpha_{last}$, of 60°) was found adequate for SNR while maintaining a ultra-low SAR.

### Ultra-low–SAR FLAIR T2-weighted and SPGR T1-weighted MR Sequences

Modifications similar to the T2-weighted sequence were also employed for optimizing the ultra-low–SAR 3D FLAIR T2-weighted sequence. Although, with FLAIR, a 180° inversion-recovery preparation pulse is used, it is turned on only once for every repetition time when whole-brain 3D acquisition is performed, and, hence, the inversion pulse is not a major SAR concern. To provide T1 contrast images, a 3D SPGR-based T1-weighted sequence was chosen that, even in a clinical version, generates lower SAR than does the spin-echo T1-weighted sequence because low–flip angle RF excitation and no refocusing pulses are involved. The sequence was further optimized for ultra-low SAR by increasing image repetition time, by stretching excitation RF pulse width to 1.9 msec, and by using 2D parallel imaging.

**Figure 1**

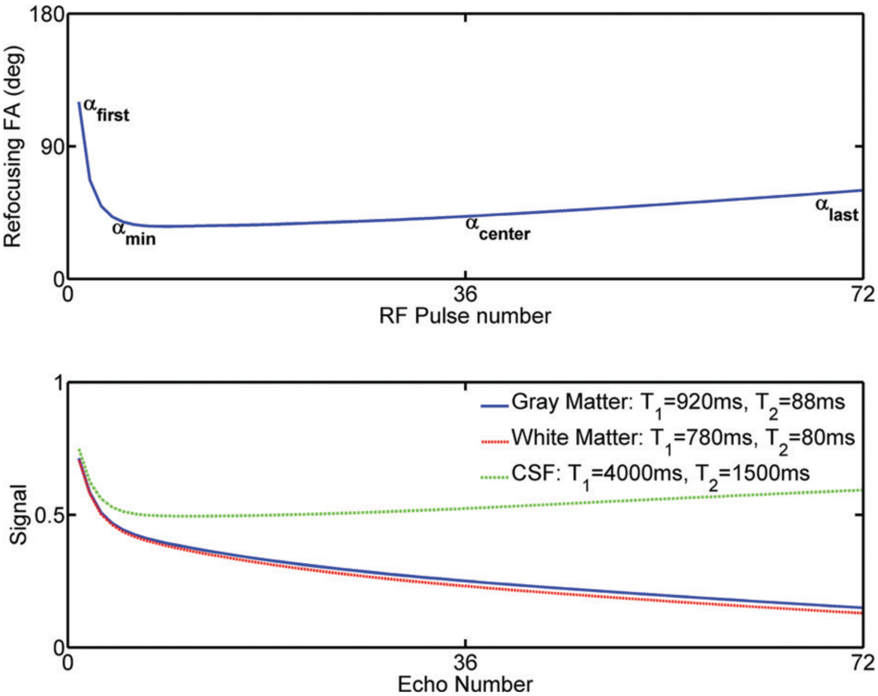


**Figure 1:** Top: Simulated optimized refocusing flip angle *(FA)* train for ultra-low–SAR 3D FSE T2-weighted sequence. Typical first ($\alpha_{first}$), minimum ($\alpha_{min}$), center ($\alpha_{center}$), and last ($\alpha_{last}$) flip angle values are included in Table 1. Bottom: Expected signal intensity *(Signal)* for cerebral tissues with typical T1 and T2 relaxation values (in milliseconds *[ms]*) at 1.5 T.

Because healthy subjects do not have known enhancing lesions, no attempt was made to compare infused contrast material sensitivity of 2D and 3D T1-weighted sequences by using gadolinium-based contrast agents in this preliminary work.

Sagittal 2D FSE T2-weighted, 2D FLAIR, and 2D spin-echo T1-weighted images obtained by using standard, high-SAR clinical protocols were also obtained with SAR levels within Food and Drug Administration–approved whole-body limits.

### SNR and CNR Calculations

For estimating the background noise under various parallel imaging and sequence conditions, a single-section noise image was obtained with the excitation RF pulse turned off and gradient hardware matched to the corresponding sequence. SNR was measured (P.M.R., S.N.S.) for every image by using a Monte Carlo method that avoids errors in noise estimates present in parallel imaging reconstruction or multicoil combination of signals (12). This method determines the true signal fluctuations and, hence, SNR on a pixel-by-pixel basis from measured characteristics of the actual thermal noise present at image acquisition and from the specific knowledge of the image reconstruction algorithm. The same method was also applied to all clinical sequences. SNR maps averaged for 4.8-mm equivalent 3D image sections were directly compared with those from the 4.8-mm 2D sagittal images obtained by using the high-SAR clinical sequences.

The mean SNR in five cerebral tissue regions was obtained by placing regions of interest at those tissue locations in the whole-brain SNR maps and averaging across all subjects. The mean CNRs were computed by subtracting adjacent tissue SNR for each subject, followed by averaging the CNR over all subjects (method design by S.N.S, D.B.H.). The tissues included were cortical gray matter (GM) and subcortical white matter (WM) in lateral, frontotemporal, and

Radiology

**Table 2**

**SNR and CNR Values from Various Tissues for Clinical 2D High-SAR and 3D Ultra-low–SAR Sequences**

| | T2 FSE | | T2 FSE FLAIR | | | |
|---|---|---|---|---|---|---|
| SNR and CNR* | 2D High SAR | 3D Ultra-low SAR | 2D High SAR | 3D Ultra-low SAR | T1 2D High-SAR Spin Echo | T1 3D Ultra-low–SAR SPGR |
| SNR | | | | | | |
| Cortical GM | 135 ± 6† | 87 ± 6 | 42 ± 6 | 66 ± 7‡ | 64 ± 4 | 78 ± 6‡ |
| Subcortical WM | 105 ± 3† | 59 ± 6 | 29 ± 2 | 43 ± 8‡ | 77 ± 2 | 115 ± 16‡ |
| Sulcal CSF | 400 ± 16† | 299 ± 17 | 13 ± 1† | 4 ± 1 | 35 ± 5 | 40 ± 5 |
| Corpus callosal WM | 85 ± 5† | 55 ± 9 | 24 ± 4 | 33 ± 4‡ | 64 ± 3 | 96 ± 10‡ |
| Ventricular fluid | 261 ± 14† | 232 ± 21 | 10 ± 3† | 1 ± 0.4 | 28 ± 1 | 29 ± 3 |
| CNR | | | | | | |
| Cortical GM–subcortical WM | 30 ± 6 | 28 ± 2 | 13 ± 8 | 23 ± 10 | 13 ± 4 | 37 ± 10‡ |
| Cortical GM–sulcal CSF | 265 ± 15† | 212 ± 17 | 29 ± 7 | 62 ± 7‡ | 29 ± 6 | 38 ± 4 |
| Corpus callosal WM–ventricular fluid | 176 ± 9 | 177 ± 15 | 14 ± 6 | 32 ± 4‡ | 36 ± 2 | 67 ± 9‡ |

Note.—Data are means ± standard deviations. T1 = T1 weighted, T2 = T2 weighted.

* SNR and CNR values are for 4.8-mm sections from 2D (high-SAR) sequences and for 4.8-mm reconstructed sections from 3D (ultra-low–SAR) sequences.

† The mean difference between 2D and 3D sequences was significant ($P < .05$), favoring a higher mean value for 2D.

‡ The mean difference between 2D and 3D sequences was significant ($P < .05$), favoring a higher mean value for 3D.

parietal locations; the corpus callosal white matter (CC WM); the sulcal cerebrospinal fluid (CSF); and the ventricular fluid (Table 2).

### Statistical Analysis

No specific statistical distribution was assumed for the tissue SNR and CNR values. To compare image quality between high-SAR 2D and ultra-low–SAR 3D methods, we separately analyzed the differences in tissue SNR and differences in tissue CNR for all seven subjects by using the Wilcoxon signed-rank test. A total of 15 separate signed-rank tests for SNR and nine separate tests for CNR were performed without Bonferroni correction at a significance level of $P = .05$. Inferences were drawn to assess the significant differences in SNR, as well as CNR differences between the high-SAR 2D and ultra-low–SAR 3D techniques (S.N.S., D.B.H.), in consultation with the biostatistician. Note that one could instead use parametric approaches if a large number of subjects were tested, satisfying normal distribution, or use a transformation toward normality.

## Results

The simulated signals in Figure 1 demonstrate sustained signal levels owing to compensated T2 decay for GM, WM, and CSF. Notice that the signal differential (and hence tissue contrast) for the GM and WM in this optimization scheme with the 3D FSE sequence is somewhat limited, while CSF intensity is moderately high. The 3D FLAIR T2-weighted sequence follows similar simulation curves by using the same refocusing flip angles, although longer echo train length and effective echo time are preferred (Table 1). Figures 2–4 show the high-SAR 2D and ultra-low–SAR 3D T2-weighted, FLAIR, and T1-weighted images for a typical subject from the volunteer group.

### Qualitative Observations

Images from both ultra-low– and high-SAR sequences were qualitatively comparable, as per assessment by a senior neuroradiologist (D.B.H., with 25 years of experience) in regard to tissue signal intensity, relative tissue contrast, and the overall image appearance, as can be seen on the images from a typical subject (Figs 2–4).

The 3D images showed fine anatomic structures, with no noticeable artifacts or loss of detail in spite of the ultra-low–SAR implementation or accelerated autocalibrating reconstruction for Cartesian sampling reconstructions. There were no noticeable alterations in tissue contrast across the whole brain owing to potential contributions from stimulated echoes or owing to the chosen RF modulation scheme and 2D accelerations. The ultra-low–SAR 3D images demonstrated slightly attenuating fat signal, compared with the high-SAR images.

### Quantitative Comparisons

Regions of interest placed in WM, GM, CSF, and ventricular fluid regions in the whole-brain SNR maps directly rendered absolute tissue SNR and CNR values for computing group averages (S.N.S. and P.M.R.) (Table 2). The standard deviations for most tissues seemed to be small (< 5% to 10%) except for fluids. Note that conventional region-of-interest–based background noise analysis for SNR and CNR estimates are usually not accurate for multicoils with parallel imaging conditions (12).

Statistical comparison of the signals from several brain tissues (S.N.S., D.B.H.), in consultation with the biostatistician, revealed the following: For SNR, *(a)* the high-SAR 2D T2-weighted sequence produced somewhat higher SNR values for all the tissues tested, compared with the ultra-low–SAR 3D sequence, although the 3D SNR values were acceptable; *(b)* SNR values with the FLAIR sequence for all the tissues (except fluids) were higher for the 3D than for the 2D technique, and one may observe that a lower SNR for fluids, as

**Figure 2**

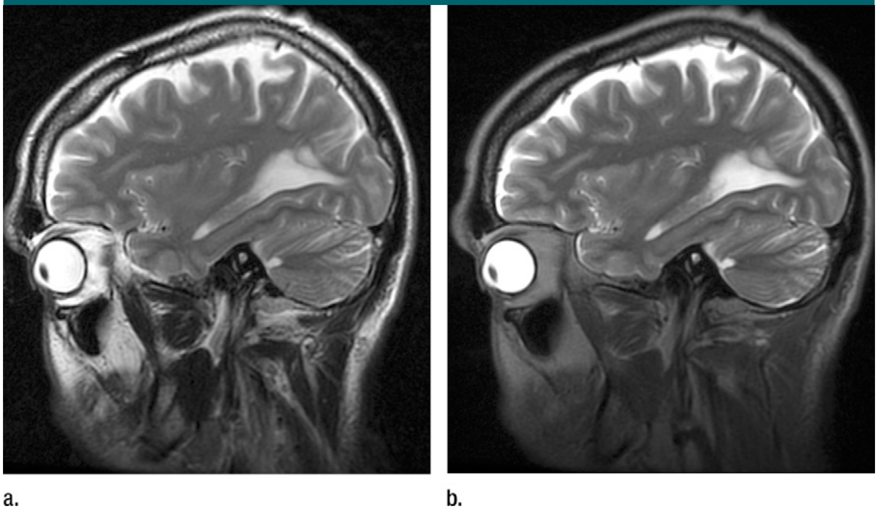

**Figure 2:** **(a)** Typical 4.8-mm directly acquired right parasagittal image section obtained with high-SAR 2D FSE clinical T2-weighted sequence and **(b)** 4.8-mm-thick section (reconstructed from three 1.6-mm sections) obtained with ultra-low–SAR 3D FSE T2-weighted sequence. Both images were acquired with 0.8 × 1.0 mm$^2$ in-plane resolution in a 40-year-old male subject.

**Figure 3**

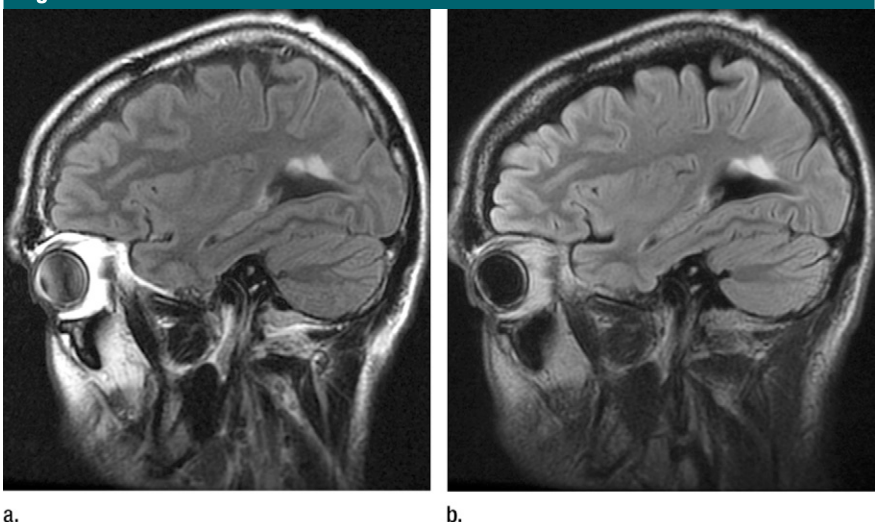

**Figure 3:** **(a)** Typical 4.8-mm directly acquired right parasagittal image section obtained with high-SAR 2D clinical FLAIR sequence and **(b)** 4.8-mm-thick section (reconstructed from three 1.6-mm sections) obtained with ultra-low–SAR 3D FSE FLAIR sequence. Both images were acquired with 0.8 × 1.0 mm$^2$ in-plane resolution in the same subject as in Figure 2.

is the case with the ultra-low–SAR 3D method, is in fact desirable; and *(c)* the SNR values for all tissues (except fluids) were higher with the ultra-low–SAR 3D SPGR T1-weighted sequence than with the high-SAR 2D spin-echo T1-weighted sequence. The signal intensity of CSF and ventricular fluid was similar for both.

For CNR, *(a)* the CNR for cortical GM–subcortical WM in T2-weighted and FLAIR sequences and the T2-weighted CNR for CC WM–ventricular fluid were similar for both 2D and 3D techniques, while for the cortical GM-CSF, the T2-weighted CNR was somewhat higher with the 2D technique than it was with the 3D technique; *(b)* the 3D FLAIR sequence produced higher CNR in cortical GM–CSF and in CC WM–fluid than did the 2D technique; and *(c)* the ultra-low–SAR 3D SPGR T1-weighted sequence produced higher CNR values for all tissue comparisons than did the 2D spin-echo T1-weighted sequence, except for cortical GM–CSF.

Although some of the mean differences are significant, as noted in Table 2, the overall SNR and CNR values, as well as the visual inspection of the images (D.B.H, N.M.R., S.N.S.), showed that the image contrast properties of the 3D approaches were quite similar to those of the 2D methods for the FLAIR and T2-weighted sequences. The 3D SPGR T1-weighted images differed visibly from the 2D spin-echo T1-weighted images, with somewhat higher image contrast on 3D T1-weighted images for most tissues. Overall, these ultra-low–SAR 3D sequences appear to represent acceptable alternatives to conventional 2D methods when minimizing SAR is important to safely offer MR imaging for clinical diagnostics.

## Discussion

We demonstrated the feasibility of ultra-low–SAR 3D imaging at 1.5 T with two orders of magnitude reduction in SAR, within a clinically feasible imaging time, resulting in SNR and CNR comparable to those of the high-SAR clinical 2D sequences. This dramatic reduction of SAR was achieved with known, but perhaps not widely appreciated, strategies to reduce the power deposition of clinical imaging sequences. That SAR can be so greatly decreased indicates that SAR reduction below regulatory maxima has not been a past focus of development. Note that the software SAR estimates used to estimate RF power deposition can vary considerably across imagers (13), probably caused by differences in SAR monitor calibrations or added safety factors. Such uncertainty in safety factors was one motivation for us to assess the feasibility of dramatically decreasing power so that a wider safety margin can be offered whenever low-SAR imaging is strongly recommended.

**Figure 4**

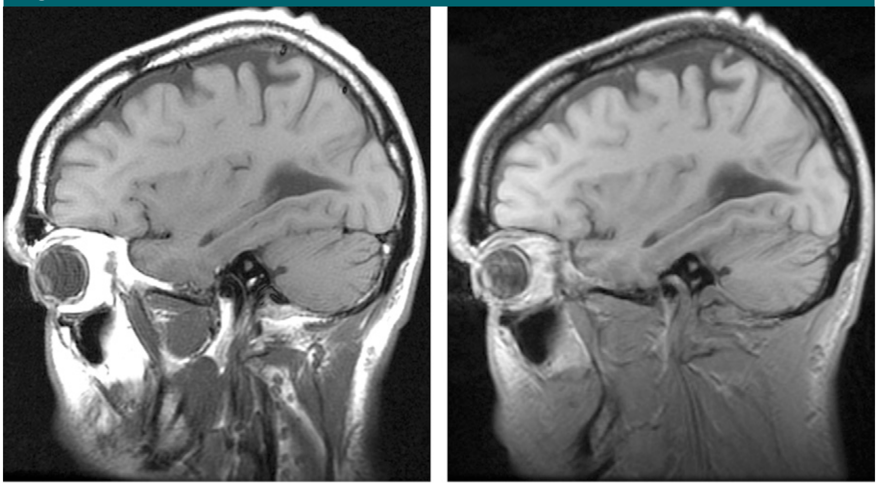

a. b.

**Figure 4:** **(a)** Typical 4.8-mm directly acquired right parasagittal image section obtained with high-SAR 2D clinical spin-echo T1-weighted sequence and **(b)** 4.8-mm-thick section (reconstructed from three 1.6-mm sections) obtained with ultra-low–SAR 3D SPGR T1-weighted sequence. Both were acquired with 0.8 × 1.0 mm$^2$ in-plane resolution from the same location and in the same subject as in Figures 2 and 3.

The relative SAR benefits of the modified 3D sequences over conventional 2D sequences, demonstrated here as two orders of magnitude, are likely to be more important than the absolute SAR values. However, if local tissue heating must be measured, calorimetric experiments should be performed to estimate local SAR more accurately.

Current safety guidelines on several implanted devices limit imaging to the use of transmit-receive head coils. The growing population of subjects with implants that may not be compatible with standard MR imaging protocols suggests that reduction of SAR and other sources of MR imaging incompatibility should receive greater attention. While it is, of course, preferable that all devices be completely MR imaging compatible, compatibility with standard high-SAR protocols may not be feasible for many devices. For example limitation to transmit-receive head coils is part of the manufacturer's guideline for imaging of deep brain stimulators (14). This restriction is motivated by an attempt to reduce RF application to extracranial components of such devices (15,16). The trend to use higher-field-strength magnets will impose further constraints on choice of advanced protocols that can be performed with conventional sequences. Our approach, with the use of dramatically lower SAR, may offer a potential solution to these problems in the future.

The results in this work are just a first step toward broader MR imaging compatibility and should not be interpreted as proof of safety for use in patients in whom imaging is limited to low-SAR approaches. The relationship between whole-body SAR and local SAR near a conductor depends on the experimental geometry and tissue properties surrounding the conductor, and these factors have not been evaluated in this study. Indeed, use of our ultra-low–SAR sequences with body coil transmission would violate current guidelines for some implants (14,17) that specify a transmit-receive head coil only, and we do not suggest or recommend this use, at least until further testing by the manufacturer or another expert party has been performed. An additional concern is that current vendor implementations of SAR estimation are not consistent across imagers, and they do not automatically provide safeguards for restricting RF power for particular devices. In our study, we have not evaluated additional factors in compatibility of implants, especially the effects of rapidly changing gradient fields and, of course, any forces or direct effects from the main magnetic field on conductors and electronics. However, if these issues are addressed by future testing and development, it seems likely that the 100-fold reduction of SAR made possible by ultra-low–SAR imaging sequences, such as those reported here, will enable greater flexibility for MR imaging compatibility and image quality.

In this preliminary work, we have not demonstrated diagnostic equivalence for pathologic findings between low- and high-SAR sequences. However, when applied to patients with multiple sclerosis, a 3D sampling perfection with application optimized contrasts using different flip angle evolutions version of FLAIR and T2-weighted sequences (SPACE; Siemens, Erlangen, Germany), which is similar to single-slab 3D FSE (Cube; GE Healthcare, Milwaukee, Wis) with reduced refocusing flip angles at 3.0 T, has demonstrated adequate lesion visualization comparable to that on 2D images (18,19). Because our results showed that the ultra-low–SAR approach essentially reproduced the SNR and CNR of the standard clinical images over a range of tissues with significantly varying T1 and T2 relaxation times, one may expect this strategy to produce satisfactory results in patients, although this hypothesis will have to be tested.

Note that because of the small number of subjects involved, we had no reliable way of assessing normality for tissue SNR and CNR values. We used nonparametric inference tests as a logical alternative, although in this situation, nonparametric tests are not ultra powerful either. As noted in the SNR and CNR values in Table 2, the ultra-low–SAR 3D sequences seem to produce images that have SNR and CNR mostly equivalent to or often somewhat higher than the SNR and CNR of images produced with the high-SAR 2D sequences. While both approaches produce acceptable tissue SNR and CNR, several mean differences as mentioned in Table 2 are significant and favor the ultra-low–SAR 3D approach. This work does not address the effect of such differences in normal tissues or in pathologic findings. Also, at this time, it is unclear how the CNR will compare for gadolinium-enhanced imaging for normal or enhancing tissues by using the two T1-weighted methods. One should also note that we have not compared our ultra-low–SAR 3D SPGR T1-weighted sequence with any other 3D gradient-echo–based T1-weighted technique. The latter can be a somewhat low-SAR technique, with an approximately one order of magnitude lower SAR than with the 2D spin-echo T1-weighted sequence and may be modified by using a similar approach.

The use of a longer 3D acquisition with the low-SAR sequence might increase the frequency of motion-degraded images, particularly for patients with limited ability to cooperate. However, cooperative patients imaged with adequate attention to comfort can usually remain motionless for the relatively short incremental time required for these lower-SAR sequences. Patients who are incapable of remaining still usually will not be able to undergo examination at the somewhat shorter, routine imaging times as well. Advantages of 3D include the ability to often choose frequency encoding along the direction of maximum motion and the capability to reduce table time by reconstructing images in other planes as a substitute for the repeat imaging in different planes, as is often performed in clinical 2D MR imaging. In addition, modern motion correction techniques are more effective with 3D acquisitions. One such method, which could be added to the existing protocol, requires essentially zero additional power and has demonstrated excellent suppression of motion artifacts with 3D FSE and 3D T1-weighted images (20).

In summary, this work has demonstrated that a 100-fold reduction in SAR of standard clinical brain protocols is achievable with image quality comparable to that of current high-SAR sequences. Following careful further in vitro and in vivo tests, these methods may provide a high-quality alternative when conventional MR imaging is contraindicated owing to high-SAR levels present in routine clinical imaging.

**Acknowledgments:** The authors thank Robert Marquis, RT(R), MR, Sue La Ruche, RT(R), MR, and Fotini Kourtelidis, RT(R), MR, for their help and also thank Efstathios Papavassiliou, MD, Rafeeque Bhadelia, MD for clinical, and Shiva Gautam, PhD, for valuable statistical discussions.

## References

1. Oshio K, Jolesz FA, Melki PS, Mulkern RV. T2-weighted thin-section imaging with the multislab three-dimensional RARE technique. J Magn Reson Imaging 1991;1(6):695–700.
2. Williams CF, Redpath TW, Smith FW. The influence of stimulated echoes on contrast in fast spin-echo imaging. Magn Reson Imaging 1996;14(4):419–428.
3. Mugler J, Kiefer B, Brookman J. Three-dimensional T2-weighted imaging of the brain using very long spin-echo trains [abstr]. In: Proceedings of the Eighth Meeting of the International Society for Magnetic Resonance in Medicine. Berkeley, Calif: International Society for Magnetic Resonance in Medicine, 2000; 687.
4. Busse RF, Brau AC, Vu A, et al. Effects of refocusing flip angle modulation and view ordering in 3D fast spin echo. Magn Reson Med 2008;60(3):640–649.
5. Hennig J. Multiecho imaging sequences with low refocusing flip angles. J Magn Reson 1988;78(3):397–407.
6. Hennig J, Weigel M, Scheffler K. Calculation of flip angles for echo trains with predefined amplitudes with the extended phase graph (EPG)-algorithm: principles and applications to hyperecho and TRAPS sequences. Magn Reson Med 2004;51(1):68–80.
7. Mugler J, Wald L, Brookman J. T2-weighted 3d spin-echo train imaging of the brain at 3 Tesla: reduced power deposition using low flip-angle refocusing RF pulses [abstr]. In: Proceedings of the Ninth Meeting of the International Society for Magnetic Resonance in Medicine. Berkeley, Calif: International Society for Magnetic Resonance in Medicine, 2001; 438.
8. Alsop DC. The sensitivity of low flip angle RARE imaging. Magn Reson Med 1997;37(2):176–184.
9. Lebel RM, Wilman AH. Time-efficient fast spin echo imaging at 4.7 T with low refocusing angles. Magn Reson Med 2009;62(1):96–105.
10. Beatty P, Brau A, Chang S, et al. A method for autocalibrating 2D-accelerated volumetric parallel imaging with clinically practical reconstruction times [abstr]. In: Proceedings of the Fifteenth Meeting of the International Society for Magnetic Resonance in Medicine. Berkeley, Calif: International Society for Magnetic Resonance in Medicine, 2007; 1749.
11. Bottomley PA, Redington RW, Edelstein WA, Schenck JF. Estimating radiofrequency power deposition in body NMR imaging. Magn Reson Med 1985;2(4):336–349.
12. Robson PM, Grant AK, Madhuranthakam AJ, Lattanzi R, Sodickson DK, McKenzie CA. Comprehensive quantification of signal-to-noise ratio and *g*-factor for image-based and *k*-space-based parallel imaging reconstructions. Magn Reson Med 2008;60(4):895–907.
13. Baker KB, Tkach JA, Phillips MD, Rezai AR. Variability in RF-induced heating of a deep brain stimulation implant across MR systems. J Magn Reson Imaging 2006;24(6):1236–1242.
14. MRI Guidelines for Medtronic Deep Brain Stimulation Systems. 1-20:M925038A001. Minneapolis, Minn: Medtronic, 2006.
15. Baker KB, Tkach JA, Nyenhuis JA, et al. Evaluation of specific absorption rate as a dosimeter of MRI-related implant heating. J Magn Reson Imaging 2004;20(2):315–320.
16. Rezai AR, Finelli D, Nyenhuis JA, et al. Neurostimulation systems for deep brain stimulation: in vitro evaluation of magnetic resonance imaging-related heating at 1.5 tesla. J Magn Reson Imaging 2002;15(3):241–250.
17. Tagliati M, Jankovic J, Pagan F, et al. Safety of MRI in patients with implanted deep brain stimulation devices. Neuroimage 2009;47(Suppl 2):T53–T57.
18. Tetzlaff RH, Mader I, Küker W, et al. Hyperecho-turbo spin-echo sequences at 3T: clinical application in neuroradiology. AJNR Am J Neuroradiol 2008;29(5):956–961.
19. Mills RJ, Young CA, Smith ET. 3D MRI in multiple sclerosis: a study of three sequences at 3 T. Br J Radiol 2007;80(953):307–320.
20. White N, Roddey C, Shankaranarayanan A, et al. PROMO: Real-time prospective motion correction in MRI using image-based tracking. Magn Reson Med 2010;63(1):91–105.